Heat Mass Transfer (2015) 51:251–263
DOI 10.1007/s00231-014-1413-2

ORIGINAL

Investigation of thermal performances of "S-shaped" enhancement elements by response surface methodology

Sendogan Karagoz

Received: 2 August 2013 / Accepted: 1 July 2014 / Published online: 15 July 2014

Abstract Electronic equipment generally uses heat sinks as cooling devices in order to effectively control heat arising from them. The heat sinks are commonly installed in the restricted space of the systems and their thermal performance can be improved both by enhancing the heat transfer rate and by reducing the friction factor. In the present work, a study is made to investigate the thermal performance characteristics of "S-shaped" enhancement elements. Response surface methodology is used to plan and analyze the experiments. The element height, the transverse pitch, the element radius, and the Reynolds number are chosen as variables to study the thermal performance in terms of the Nusselt number and the friction factor. In order to verify the adequacy of the model used, confirmation experiments are performed on the experimental setup. The experimental results indicate that the model used in this study is reasonable and accurate and can be used for determining the Nusselt number and the friction factor with the limitations of the factors analyzed.

1 Introduction

Electronic equipment generally uses heat sinks as cooling devices in order to effectively control heat arising from them. The heat sinks are commonly installed in the restricted space of the systems and their thermal performance can be improved both by enhancing the heat transfer rate and by reducing the friction factor. Moreover, the advancement of packaging technologies has led the size of heat sinks miniaturized. Therefore, the optimal design of heat sinks is becoming more and more important issue and is one of interesting research areas; thereby it has been much paid attention by numerous researchers [1–12].

Approximation models such as the sequential approximate optimization (SAO) technique have been used in order to optimize design of fluids/thermal (FT) systems. Generally, the SAO is classified into two categories according to information required during the optimization: gradient-based approximation (GBA) and function-based approximation (FBA). In the GBA, gradient information for objective functions and/or constraints are required to approximate the optimization problem. However, it is often unavailable and sometimes too expensive to approximate through the finite difference method because the analysis of design sensitivity has to be performed. Thus, in particular optimization problems the GBA cannot be applicable to optimize the FT-system. In contrast to the GBA, the FBA only needs the function for optimization and is relatively simple in the approximate optimization problem. The most widely used methodology in the FBA is the response surface approximation (RSA) related to the trust region algorithm and the design of experiments [7, 13, 14].

The literature reveals that response surface methodology (RSM) has been widely used in numerous fields for optimization design [15–21]. However, very little effort is reported on the use of RSM in the optimization of heat-sinks [7–9, 22].

Park and Moon [7] obtained numerically the optimal values of the design variables which minimize the pressure loss under the required temperature rise in a plate-fin heat sink. The sequential approximate optimization (SAO) algorithms were used. The researchers proposed the progressive quadratic response surface method (PQRSM), which is one of the SAO algorithms, for constrained

S. Karagoz (✉)
Department of Mechanical Engineering, Engineering Faculty, Atatürk University, Erzurum, Turkey
e-mail: skaragoz@atauni.edu.tr

nonlinear optimization problems for the optimization of heat sink. The optimal solutions obtained from the PQRSM were compared with those of the sequential quadratic programming (SQP) method, which is one of the gradient-based optimization algorithms, to validate the efficiency and fidelity of the PQRSM.

Sahin and Demir [10, 11] investigated performance analysis of a heat exchanger having perforated pin fins and perforated square fins using the Taguchi experimental design method. Optimum design parameters and their levels were investigated. Nusselt number and friction factor were considered as performance parameters. An L_9 (3^3) orthogonal array was selected as an experimental plan. First of all, each goal was optimized separately. Then, all the goals were optimized together, considering the priority of the goals.

For investigating the influences of designing parameters of parallel-plain fin heat sink with an axial-flow cooling fan on the thermal performance, a systematic experimental design based on the response surface methodology was used [8]. The thermal resistance and pressure drop were adopted as the thermal performance characteristics. The most significant influential factors for minimizing thermal resistance and pressure drop were identified from the analysis of variance. The optimum designing parameters, which are based on the quadratic model of RSM and the sequential approximation optimization method, are found to be fin height of 60 mm, fin thickness of 1.07 mm, passage width between fins of 3.32 mm, and distance between the cooling fan and the tip of fins of 2.03 mm.

Chiang et al. [8] used the RSM to identify the effects of design parameters of the pin–fin heat sink on the thermal performance. The height and diameter of pin–fin and the width of pitch between fins were selected as design parameters. The thermal resistance (R_{th}) and pressure drop (ΔP) were adopted as the thermal performance characteristics. An effective procedure of RSM was established for predicting and optimizing the thermal resistance (R_{th}) and the pressure drop (ΔP) of pin–fin heat sink with the design constraints.

An experimental study was made in order to determine flow and heat transfer characteristics of metallic honeycombs structures that are used in compact heat exchangers [22]. Design parameters and values were selected for fin height (H) 20, 40 and 60 mm, for fin thickness (t) 6, 10 and 15 mm, for distance between fins (S_y) 20, 30, 40 mm, for angle (φ) 0°, 15° and 30° and for Reynolds number (*Re*) 8,000, 16,000 and 25,000. With the help of RSM, mathematical models were established for Nusselt number, thermal resistance and friction factor. Multiobjective optimization was also made in order to determine the design parameters giving minimum thermal resistance and friction factor.

In the present work, an experimental study is made in order to determine flow and heat transfer characteristics of "S-shaped" enhancement elements. Response surface methodology is used to plan and analyze the experiments. The element height (H), the transverse pitch (S_y), the element radius (R), and the Reynolds number (*Re*) are chosen as variables to study the thermal performance in terms of the Nusselt number and the friction factor. A predictive model for thermal performance characteristics is created by using the RSM.

2 Response surface methodology

The response surface methodology (RSM), firstly induced by Box and Wilson [23], is a sequential experimentation strategy for building and optimizing the empirical model. RSM is a collection of mathematical and statistical procedures that are useful for the modeling and analysis of problems in which response of demand is affected by design parameters, and the objective is to optimize the design parameters on the desired value of the response function. Through using the design of experiments and applying regression analysis, the modeling of the desired response to the several independent input variables can be gained [9, 24, 25].

In the RSM, the quantitative form of relationship between desired response and independent input variables could be represented as

$$y = f(x_1, x_2, x_3, \ldots, x_n) \pm \varepsilon \tag{1}$$

where y is the desired response, f is the response function (or response surface), x_1, x_2, x_3, …, x_n are the independent input variables, and ε is the fitting error [9].

In most RSM problems, the form of the relationship between response and the independent variables is unknown. Thus, the first step in RSM is to find a suitable approximation for the true functional relationship between the response and the independent variables. If the response can be well modeled by a linear function of the independent variables, the function [Eq. (1)] can be written as:

$$y = a_o + \sum_{i=1}^{n} a_i x_i \pm \varepsilon \tag{2}$$

However, if system can't be modeled by using a linear function, a higher order polynomial such as the quadratic model [Eq. (3)] or exponential model or logarithmic model may be used:

$$y = a_o + \sum_{i=1}^{n} a_i x_i + \sum_{i=1}^{n} a_{ii} x_i^2 + \sum_{i<j}^{n} a_{ij} x_i x_j + \varepsilon \tag{3}$$

where a_i represents the linear effect of x_i, a_{ii} represents the quadratic effect of x_i and a_{ij} reveals the linear-by-linear interaction between x_i and x_j. Then response surface f

contains the linear terms, squared terms and cross product terms [9, 15].

The response surface method is a sequential process and its procedure can be summarized as shown in Fig. 1.

3 Experimental details

3.1 Experimental set-up

In the experimental studies, a fan-driven wind tunnel operating in suction mode, and positioned horizontally was used. A schematic display of the experimental setup is shown in Fig. 2. The experimental set-up mainly consisted of a main duct, test section and S-shaped elements. The main duct was constructed of wood of 18 mm thickness and had an internal cross-section of 112 mm width and 60 mm height. A bell-mouth section was fitted at the entrance of the wind tunnel. The test section had a cross section of 112 mm × 60 mm and a length of 440 mm. Before the test section, a space with a length of 1,320 mm was allocated as an entrance region in order to assure a fully developed flow in the test section. The outer surfaces of the wind tunnel were covered with a layer of glasswool to ensure good insulation against heat losses to the ambient air.

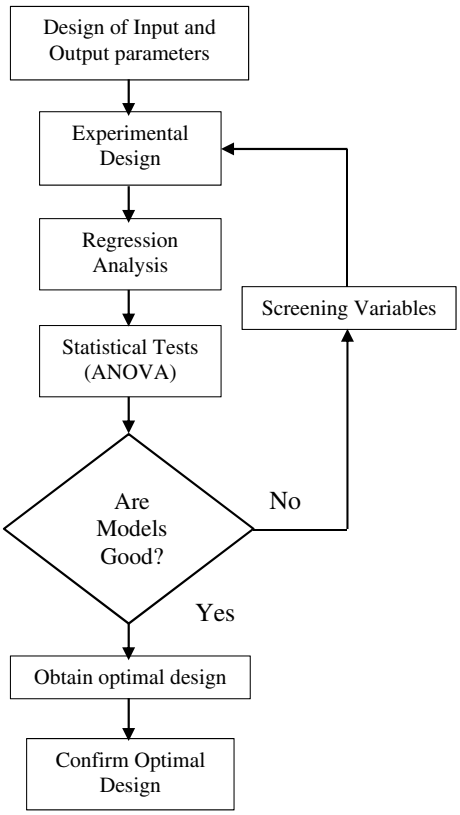

Fig. 1 Procedure of response surface methodology [15]

An aluminum plate (Al 1050) with a dimension of 111 mm × 242 mm and 6 mm in thickness was used as the base plate (Fig. 3). A heat sink compound was applied between the base plate and the heater and also the base plate and the bottoms of the S-shaped elements so as to reduce contact resistances.

The heating unit mainly consisted of an electrical heater, a firebrick and a thermal insulation was replaced in an 18 mm thick wooden box covered by a glasswool with a thickness of 15 mm (Fig. 3). A plate electric heater having same dimensions with the base plate, controlled by a variac was placed under the base plate to obtain a constant heat flux throughout the base plate. The firebrick was placed under the heater. The bottom and lateral surfaces of the firebrick were insulated using rockwool. In order to accomplish constant heat flux thermal boundary condition, electrical power supplied to electric heater was fixed at 40 W with a Hioki 3333 wattmeter and a controllable variac. This heat input was equal to a heat flux of 1,515 W/m^2.

"S-shaped" elements, made of aluminum were used for enhancing convective heat transfer (Fig. 4). Aluminum (Al 3000) was selected as the S-shaped element material taking into considerations of the thermal conductivity, machinability and cost. S-shaped elements with different heights (H) corresponding to H values of 20, 30 and 40 mm, and with different distance between the S-shaped elements (S_y) corresponding to S_y values of 7, 18 and 29 mm were used (Fig. 4; Table 1). To fabricate the test elements, "S-shaped" were cutted to the sizes specified in the test plan (Tables 1, 2).

The steady-state surface temperature of the base plate was measured by eight T-type (copper–constantan, 0.25 inner diameter) thermocouples spread over the base plate surface (Fig. 5). The average of these readings was taken as the steady-state temperature of the test surface. The inlet temperature of the air stream was measured using a T-type thermocouple while the outlet temperature was determined as the average reading of the temperatures measured from two T-type thermocouples. Furthermore, one thermocouple for the outer surface temperature of the heating section and one for the ambient temperature were employed. Therefore, totally 13 T-type thermocouples were used to obtain steady-state temperatures of the system. The readings of the thermocouples were recorded using a computer via a PCLD-HG 818 data acquisition card. All the thermocouples were calibrated to ±0.1 °C deviation between 15 and 90 °C with 5 °C intervals by employing a PolyScience thermostat before the experiments.

The pressure drop along the test section was measured via two static-pressure taps placed at the bottom of the

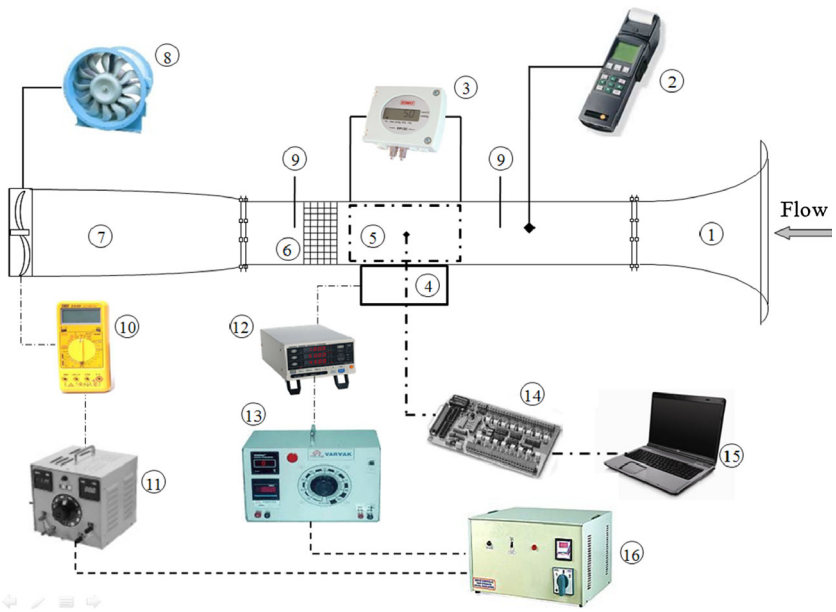

(1) effuser
(2) anemometer
(3) differential pressure transducer
(4) heating unit
(5) test section
(6) mixer
(7) diffuser
(8) fan
(9) inlet and outlet thermocouples
(10) multimeter
(11) variac
(12) wattmeter
(13) variac
(14) data acquisition card (DAQ)
(15) computer
(16) voltage regulator

Fig. 2 A schematic display of experimental setup

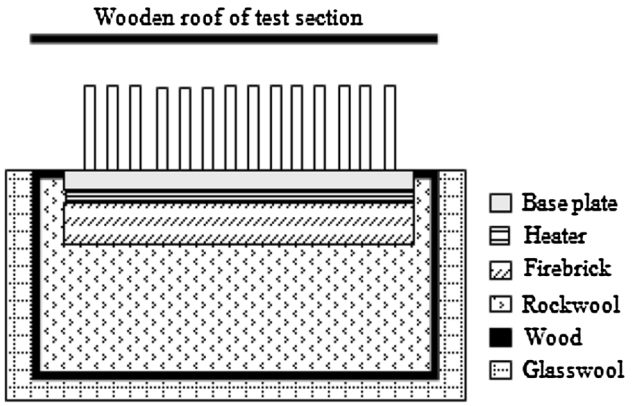

Fig. 3 A sectional view of the heating unit and test section

internal walls of the entrance and exit of the test section (Fig. 5). The pressure taps were connected to KIMO CP100 differential pressure transmitter, capable to operate between 0 and 100 Pa. The values of the pressure drop were directly read in Pa unit.

The mean inlet velocity of the air flow entering to the test section was controlled with a variac connected to the power input of the fan by changing the voltage, and measured by a TESTO 400 anemometer. Moreover, a voltage regulator was connected the system to reduce the impact of fluctuations in network.

The Reynolds numbers (*Re*) used in the experiments were 8,000, 16,000 and 25,000, which was based on the hydraulic diameter of the channel over the test section (D_h) and the average velocity (U).

If the change in temperatures read onto the test surface was almost equal to 0.5 °C or lower, the system was considered to have reached the thermal equilibrium that takes approximately (60–70 min). After having reached the thermal equilibrium, the measurements were taken and regarded as steady state values of the system.

3.2 Performance characteristics

Improvement of thermal performance for a heat transfer enhancement device can be achieved by increasing the heat transfer rate. For a given operating condition, increasing the heat transfer rate is a principal cause of high thermal performance. The average Nusselt number is regarded as the thermal performance characteristics in this study, which is defined as follows:

$$Nu = \frac{h_{av} D_h}{k} \tag{4}$$

where h_{av} is the average heat transfer coefficient, k is the thermal conductivity of air, and D_h is the hydraulic diameter of the channel.

The average heat transfer coefficient h_{av} can be expressed via

$$h_{av} = \frac{\dot{Q}_{conv}}{A_s \left[T_s - \left(\frac{T_{in} + T_{out}}{2} \right) \right]} \tag{5}$$

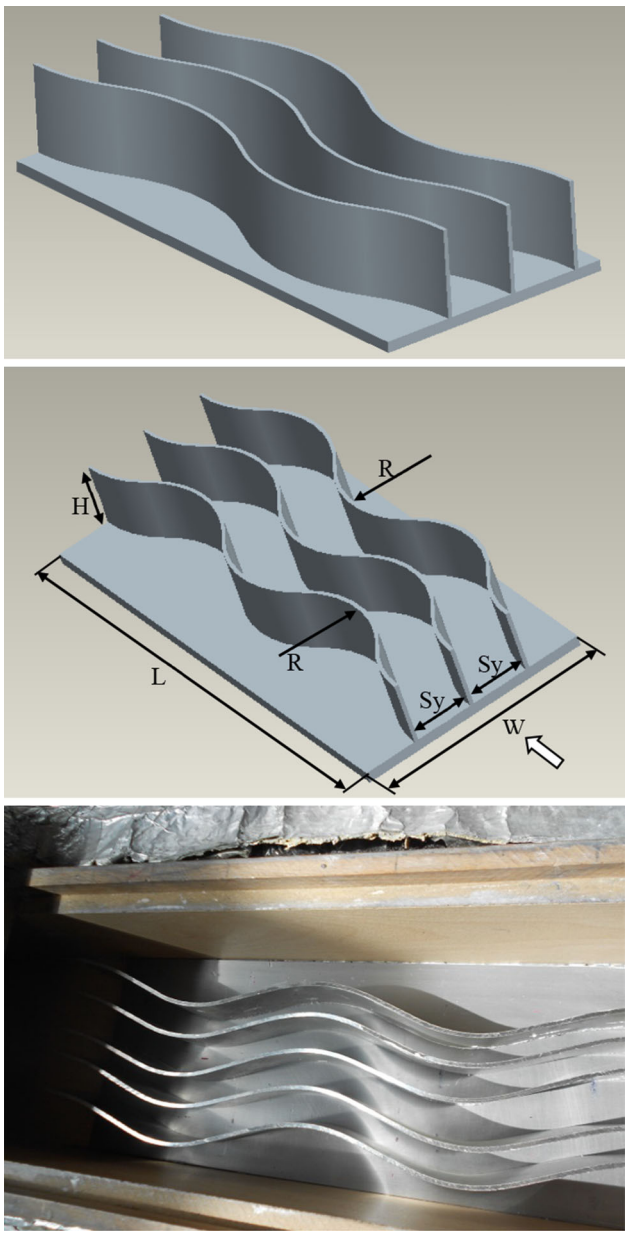

Fig. 4 The heat transfer enhancement elements used in the experimental studies

Table 1 The scheme of design parameters and their levels

Symbol	Factor	Units	Levels		
			−1	0	+1
X_1	Element height (H)	mm	20	30	40
X_2	Transverse pitch (S_y)	mm	7	18	29
X_3	Element radius (R)	°	50	85	120
X_4	Reynolds number (*Re*)		8,000	16,000	25,000

Table 2 Design of experimental matrix and results for the S-shaped elements performance characteristics

Exp. no.	Design parameters and levels				Experimental results	
	H	S_y	R	*Re*	*Nu*	f
1	20	29	120	25,000	249	0.077
2	30	18	85	16,000	298	0.291
3	40	29	120	8,000	157	0.509
4	30	29	85	16,000	214	0.160
5	30	18	85	16,000	293	0.291
6	40	29	120	25,000	284	0.133
7	30	18	85	16,000	295	0.291
8	40	29	50	25,000	347	0.138
9	20	7	50	25,000	391	0.160
10	30	18	85	8,000	227	0.622
11	20	18	85	16,000	250	0.203
12	40	7	120	25,000	513	0.283
13	30	18	120	16,000	307	0.246
14	40	29	50	8,000	217	0.520
15	20	7	120	8,000	185	0.604
16	30	18	85	16,000	296	0.291
17	40	7	120	8,000	353	1.025
18	40	7	50	8,000	373	0.752
19	30	18	85	16,000	294	0.291
20	40	7	50	25,000	575	0.274
21	30	18	85	25,000	362	0.174
22	30	7	85	16,000	350	0.431
23	20	29	50	25,000	269	0.076
24	20	29	50	8,000	160	0.322
25	20	7	120	25,000	323	0.149
26	30	18	50	16,000	343	0.275
27	30	18	85	16,000	292	0.291
28	20	7	50	8,000	208	0.614
29	40	18	85	16,000	358	0.337
30	20	29	120	8,000	139	0.318

where $\dot{Q}_{conv}$ is the convective heat transfer rate, T_s is the average surface temperature, T_{in} is the inlet air temperature, T_{out} is the outlet air temperature, and A_s is the heat transfer surface area. Either the projected or the total area of the test surface can be taken as the heat transfer surface area in the calculations. The total area is equal to the sum of the projected area and surface area contribution from the S-shaped elements. In this study, the calculations were made based on the projection area, which is equal to the multiplication of the width of the base plate (W) with length of the base plate (L).

The convective heat transfer rate from electrically heated test surface at steady state conditions is calculated by using

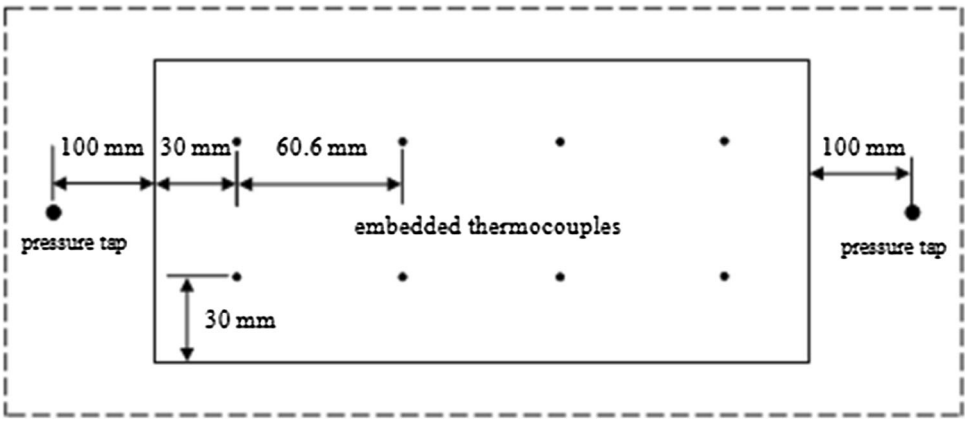

Fig. 5 Locations of surface thermocouples and pressure taps

$$\dot{Q}_{conv} = \dot{Q}_{elect} - \dot{Q}_{cond} - \dot{Q}_{rad} \tag{6}$$

where $\dot{Q}$ indicates the heat transfer rate in which subscripts conv, elect, cond, and rad denote convection, electrical, conduction, and radiation, respectively. The electrical heat input is calculated from the electrical potential and current supplied to the heater:

$$\dot{Q}_{elect} = VI \tag{7}$$

In similar studies, investigators [1, 3, 10–12, 26] reported that total radiative heat losses from a similar test surface would be about 0.5 % of the total electrical heat input. The conductive heat losses through the sidewalls can be neglected in comparison to those through the bottom surface of the test section. Using these findings, together with the fact that the two sides walls and the top wall of the test section were well insulated and readings of the thermocouple placed at the outer surface of the heating section were nearly equal to ambient temperature, one could assume with some confidence that the terms of $\dot{Q}_{cond}$ and $\dot{Q}_{rad}$ in Eq. (6) may be omitted:

$$\dot{Q}_{conv} = \dot{Q}_{elect} \tag{8}$$

Friction factor (f) is regarded as the second thermal performance characteristics, which is defined in the following:

$$f = \frac{\Delta P}{\left[\left(\frac{L}{D_h}\right)\left(\rho\frac{U^2}{2}\right)\right]} \tag{9}$$

where ΔP is the pressure drop between inlet and outlet of the test section, L is the length of the test section, D_h is the hydraulic diameter, ρ is the density of air, and U is the air velocity.

On the other hand, Reynolds number (Re) and hydraulic diameter of the channel (D_h,) can be calculated by using Eqs. (10) and (11), respectively:

$$\mathrm{Re} = \frac{UD_h}{v} \tag{10}$$

Table 3 Accuracy of instruments used in the experiments

Instruments	Type/model	Accuracy
Thermocouples	0.25 mm diameter T type copper–constantan thermocouple	± % 0.5 °C
Differential pressure transducer	KIMO CP100	±1.5 % of reading ±3 Pa
Anemometer	TESTO 400	0.2 m/s
PCL-818HG data acquisition card	Advantech	0.01 % of FSR ±1 LSB
Temperature calibrator	PolyScience	%0.1°C
Wattmeter		±0.1 %rdg +0.1 %

$$D_h = \frac{4A_c}{P} \tag{11}$$

where υ is the kinematic viscosity of air, A_c is the cross section area of the channel; P is the wet perimeter of the channel. The thermo-physical properties (k, ρ and υ) of air, those are necessary to determine Nu, Re and f, is calculated at the bulk mean temperature, which is mean of inlet and outlet temperature of air [$T_m = (T_{in} + T_{out})/2$] [27].

Accuracy of instruments used in the experiments is given in Table 3. By using the estimation method of Kline and McClintock [28], maximum uncertainties of the investigated non-dimensional parameters are found as follows: Re, 4.15 %; Nu, 7.8 %; f, 17.1 %.

3.3 Experimental conditions and plan

The standard RSM are based on three types of design of experiments (DOE) matrices, including central composites designs (CCD), Box–Behnken design (BBD) and expected integrated mean squared error optimal (EIMSE-optimal). A series of real or simulation experiments should be

implemented to obtain the values of the response variable, which can be recorded in the vector y [20]. In this study to create an accurate second-order Response Surface Model the CCD method is used. Box and Wilson first described the CCD method in 1951. Today it is one of the most popular second-order models. Each design consists of a standard first order design with n_f factorial points and n_0 center points, augmented by n_a axial points (Fig. 6). The factorial points are used to fit linear and interaction terms and the axial points provide additional levels of the factor for the purpose of estimating the quadratic terms. The resulting values, for each of the variables, are used to determine the coefficients (a_0, a_i, $a_{i,j}$) of the polynomial equation (Eq. 3) and the equation simplified according to the influence of the factors in the final response [21].

In this study, three-factor CCD model is used. The geometric and operating parameters which strongly influence the thermal performance of the S-shaped elements are the element height (H), the transverse pitch (S_y), the element radius (R) and the Reynolds number (*Re*). The levels of various design parameters and their designation is presented in Table 1. As seen, the element height (*H*), the transverse pitch (S_y), the element radius (*R*), and Reynolds Number (*Re*) selected as the design parameters. In this investigation, total 30 experiments were conducted at the stipulated conditions based on the face centered CCD. The response variables investigated are the Nusselt number (*Nu*) and the friction factor (f). The data obtained from experimental studies were analyzed using the software program so-called Design Expert 8.0.3.

4 Results and discussion

The results of the thermal performance evaluation of S-shaped elements in each experimental plan are given in Table 2. In order to test the fit of the quadratic model with the experimental data obtained in this study, the test for significance of the regression model and the test for significance on individual model coefficients are performed.

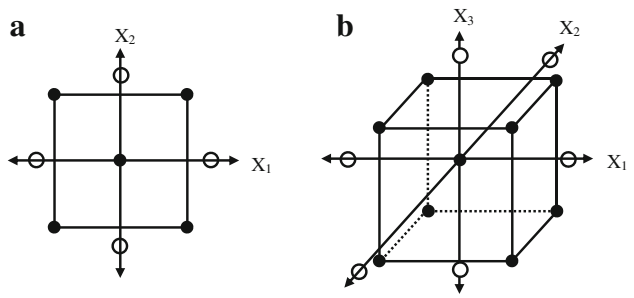

Fig. 6 **a** Two-factor central composite design model. **b** Three-factor central composite design model [21]

The analysis of variance (ANOVA) is applied to summarize the above tests performed.

4.1 Analysis of variance (ANOVA)

The results of the quadratic model for the Nusselt number in the form of ANOVA are presented in Table 4. The value of "Prob. > F" for this model in Table 4 is <0.05 (i.e. $\alpha = 0.05$, or 95 % confidence). This indicates that the model is considered to be statistically significant, which is desirable as it demonstrates that the terms in the model have a significant effect on the response. In the same manner, the main effect of factor X_1 (element height H), factor X_2 (transverse pitch S_y), factor X_3 (element radius R), factor X_4 (Reynolds number, *Re*), interaction effect of factor X_1 (element height H) with factor X_2 (transverse pitch S_y), interaction effect of factor X_1 (element height H) with factor X_4 (Reynolds number, *Re*), interaction effect of factor X_2 (transverse pitch, S_y) with factor X_4 (Reynolds number, *Re*), and interaction effect of factor X_3 (element radius, R) with factor X_4 (Reynolds number, *Re*) are the significant model terms. Other model terms is found to be insignificant effect due to their "Prob. > F" value >0.05. These insignificant model terms is eliminated.

The other important coefficient R^2 in the ANOVA table is defined as the ratio of the explained variation to the total variation and is a measure of the degree of fit. When R^2 approaches to unity, the better response model fits the actual data [9]. The value of R^2 calculated in Table 4 for this model is 0.99 and reasonably close to unity, which is acceptable. It denotes that about 99 % of the variability in the data is explained by this model. It also confirms that this model provides an excellent explanation of the relationship between the independent factors and the response (Nusselt number, *Nu*).

Another method of statistical comparison is the adjusted coefficient of determination Adj-R^2 [25]. Adj-R^2 is the percentage of the variability of the dependent variable that is explained by the variation of the independent variables after accounting for the intercept and number of independent variables. This is a number between 0 and 1. The adjusted R^2 does some adjustment for degrees of freedom. When this Adj-R^2 value approaches to unity, it means that there is good correlation between the independent input variables and the output variables. In this study, the value of Adj-R^2 is obtained as 0.9866 for the Nusselt Number, *Nu*. This value is over 0.95 and reasonably close to unity, which is acceptable. It denotes that about 98 % of variability in the data is explained by this model. It also confirms that this model provides an excellent explanation of the relationship between the independent factors and the response (*Nu*).

Table 4 ANOVA table for the Nusselt number

Source	Sum of squares	Degrees of freedom	Mean square	f-value	Prob. > F	
Model	263,000	10	26,297.35	215.25	<0.0001	Significant
X_1	53,525.71	1	53,525.71	438.13	<0.0001	
X_2	82,563.92	1	82,563.92	675.81	<0.0001	
X_3	6,833.29	1	6,833.29	55.93	<0.0001	
X_4	93,322.07	1	93,322.07	763.87	<0.0001	
X_1X_2	16,034.56	1	16,034.56	131.25	<0.0001	
X_1X_4	696.64	1	696.64	5.70	0.0275	
X_2X_4	2,911.08	1	2,911.08	23.83	0.0001	
X_3X_4	629.72	1	629.72	5.15	0.0350	
Residual	2,321.22	19	122.17			
Cor. total	265,300	29				
Standard deviation	11.05		R^2	0.9913		
Mean	297.40		Adj.-R^2	0.9866		
Coefficient of variation	3.72		Predicted R^2	0.9657		
Predicted residual of sum of squares (PRESS)	9,111.05		Adequate precision	64.916		

In addition, the large adequate precision (64.916) indicates that the regression model can be used to navigate the design space.

The ANOVA results of the quadratic mode of the friction factor are listed in Table 5. The large model f-value of 194.04 indicates the significance of the regression model. The large value of the coefficient of multiple determination ($R^2 = 0.9841$) implies that the quadratic model adequately represents the experimental results. The associate "Prob. > F" values <0.05 for this model indicate that the model terms are statistically significant and the effect of the model terms with the "Prob. > F" values >0.1 are insignificant. The value of "Prob. > F" in Table 5 for this model is also <0.05 (i.e. $\alpha = 0.05$, or 95 % confidence) indicates that the model is considered to be statistically significant. The significant model terms include the main effect of factor X_1 (element height H), factor X_2 (transverse pitch S_y), factor X_4 (Reynolds number, *Re*), interaction effect of factor X_1 (element height H) with factor X_2 (transverse pitch S_y), interaction effect of factor X_1 (element height H) with factor X_4 (Reynolds number, *Re*), and interaction effect of factor X_2 (transverse pitch S_y) with factor X_4 (Reynolds number, *Re*) are the significant model terms. Other model terms is found to be insignificant effect due to their "Prob. > F" value >0.05. These insignificant model terms is eliminated.

Furthermore, the value of adequate precision in this model, which compares the range of the predicted value at the design point to the average prediction error, is well above 4. The value of ratio is >4, which presents the adequate model discrimination.

According to the experimental results in this analysis, H, S_y, and *Re* is found to be effective on the friction factor f. The effect of element radius R on the friction factor f is found to be insignificant.

The relationship between the design parameters and the Nusselt Number, *Nu*, and the design parameters and the friction factor, f is determined using the second-degree polynomial model. The terms that are low of importance level are eliminated by "stepwise" approach contained in this mathematical model. Appropriateness of the model used in the analysis is proven by the statistical and experimental (confirmation tests) analysis. The quadratic models of response equation in terms of actual factors are expressed as:

$$\begin{aligned} Nu = {} & -6.27783 + 9.41115(H) + 11.43669(S_y) \\ & - 2.16047(R) + 0.01018(\mathrm{Re}) - 0.28788(H)(S_y) \\ & + 0.00007(H)(\mathrm{Re}) - 0.00013(S_y)(\mathrm{Re}) \\ & - 0.00002(R)(\mathrm{Re}) - 0.18540\left(S_y^2\right) + 0.01140(R^2) \end{aligned} \tag{12}$$

$$\begin{aligned} f = {} & 0.86993 + 0.02109(H) - 0.01441(S_y) - 0.00007(\mathrm{Re}) \\ & - 0.00022(H)(S_y) - 4.93871 \times 10^{-7}(H)(\mathrm{Re}) \\ & + 0.0000006(S_y)(\mathrm{Re}) + 1.53144 \times 10^{-9}(\mathrm{Re}^2). \end{aligned} \tag{13}$$

These models listed above can be used to predict the Nusselt number, *Nu* and the friction factor, f. Figures 7 and 8 displays the normal probability plots of the residuals for both Nusselt number, *Nu* and the friction factor, f,

Table 5 ANOVA table for the friction factor

Source	Sum of squares	Degrees of freedom	Mean square	f-value	Prob. > F	
Model	1.32	7	0.19	194.04	<0.0001	Significant
X_1	0.14	1	0.14	146.41	<0.0001	
X_2	0.25	1	0.25	256.37	<0.0001	
X_4	0.89	1	0.89	921.74	<0.0001	
X_1X_2	0.009665	1	0.009665	9.97	0.0046	
X_1X_4	0.030	1	0.030	31.19	<0.0001	
X_2X_4	0.060	1	0.060	61.82	<0.0001	
Residual	0.021	22	0.0009695			
Cor. total	1.34	29				
Standard deviation	0.031		R^2	0.9841		
Mean	0.34		Adj.-R^2	0.9790		
Coefficient of variation	9.21		Predicted R^2	0.9563		
Predicted residual of sum of squares (PRESS)	0.058		Adequate precision	52.005		

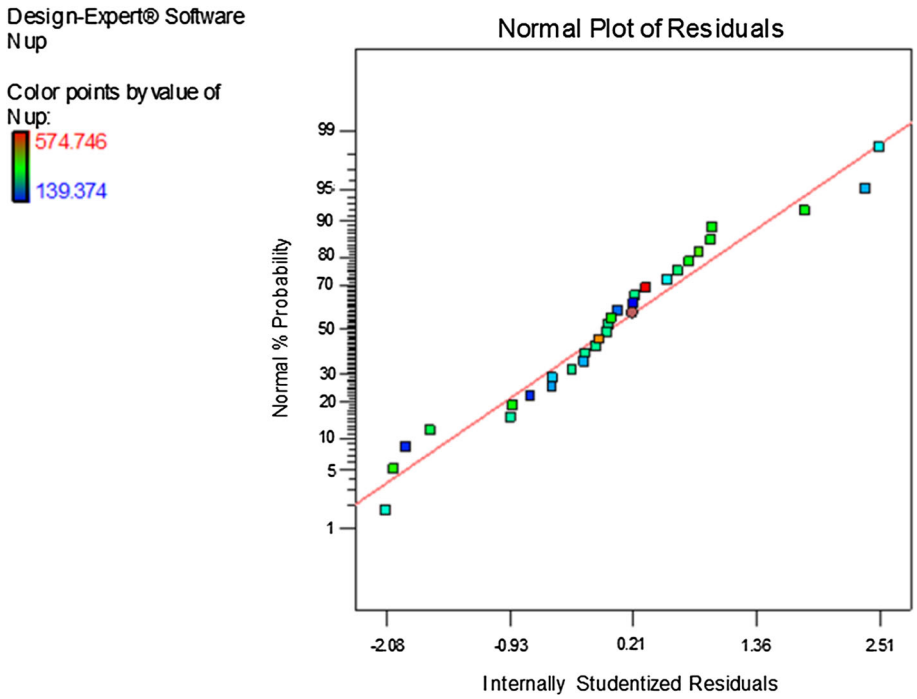

Fig. 7 Normal probability plot residuals for the Nusselt Number *Nu*

respectively. Notice that the residuals are generally falling on a straight line, which means that the errors are normally distributed. Further, it indicates that the developed regression mathematical models can yield very accurate results.

4.2 Effect of design parameters on the Nusselt number

Heat transfer enhancement with heat sink arrangements is achieved by the increase in the surface area (surface extension) and also by the turbulence (mixing) generated due to the attachments. Improved heat-transfer rates are normally accompanied by increases in the friction factor in the flow over such surfaces. Thus the main target is to design the attachments in such a way and geometry that they will yield maximum enhancement in the heat-transfer rate with minimum increase in the friction factor or minimum decrease in the flow rate [29].

The effect of Reynolds number (*Re*) on the Nusselt number (*Nu*) at various element heights (H) is presented in Fig. 9. It is seen that an increase in the Reynolds number *Re* leads to the increase of the Nusselt number (*Nu*). This figure also displays that that the effect of element height

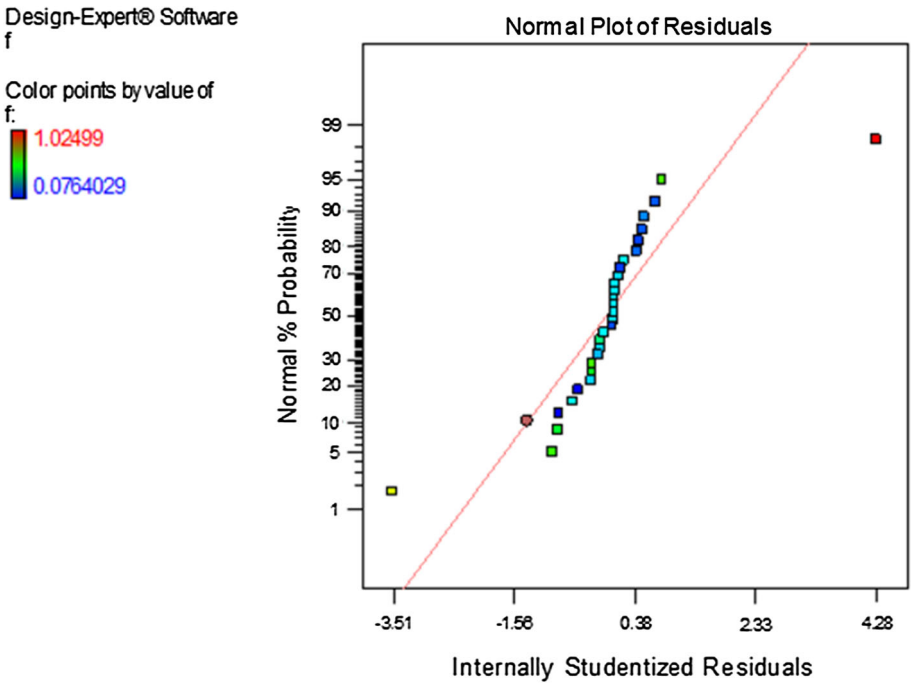

Fig. 8 Normal probability plot residuals for the friction factor (*f*)

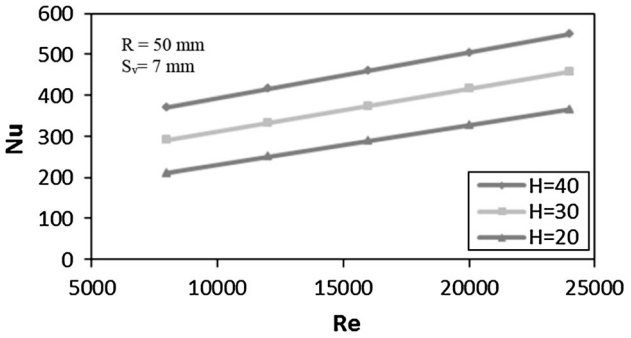

Fig. 9 The effect of Reynolds number on the Nusselt number at different element height

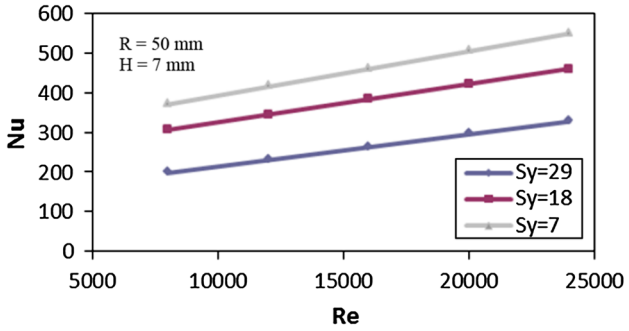

Fig. 10 The effect of Reynolds number on the Nusselt number at different transverse pitch

(H) has the similar result. Namely increasing the element height (H) increases the Nusselt number (*Nu*). The heat transfer surface area increases due to an increase in the element height H, and the flow becomes more turbulent due to a reduction in the free flow area that is a by-pass area between the channel ceiling and the edge of the S-shaped elements, and this also increases the Nusselt number *Nu*, i.e. the amount of heat taken out of the heat exchanger. These S-shaped elements not only increase the surface area, but they also increase turbulence, and induce a mixing effect inside the flow. The increase in turbulence and the induced mixing tend to increase the heat transfer coefficient.

Figure 10 shows the effect of the transverse pitch S_y on the Nusselt number *Nu*. It can be seen that increasing the transverse pitch S_y decreases the Nusselt number *Nu*. This is because an increase in the transverse pitch causes a decrease in the number of element in the channel and hence increases the dimension of gap among the elements. As a result, heat transfer surface area decreases and turbulence effect also decreases.

Figure 11 presents the effect of element radius on the Nusselt number *Nu*. An observation of Fig. 11 reveals that increasing element radius R leads to a decrease in the Nusselt number *Nu*. However, this decreasing effect is diminished for higher element radius. A decrease in the element radius R leads to an increase in turbulence, hence the Nusselt number increases.

4.3 Effect of design parameters on the friction factor

The effect of Reynolds number (*Re*) on the friction factor (f) at various element heights (H) is presented in Fig. 12. It can be seen that the friction factor f decreases with the

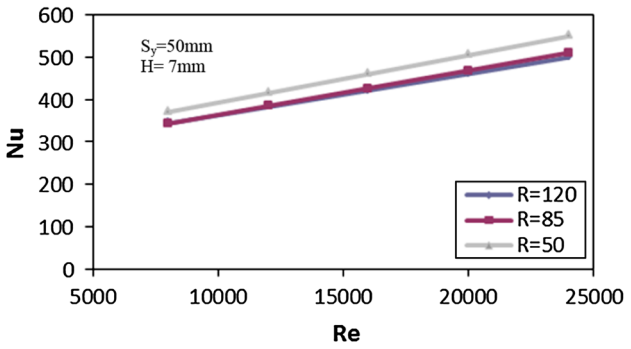

Fig. 11 The effect of Reynolds number on the Nusselt number at different element radius

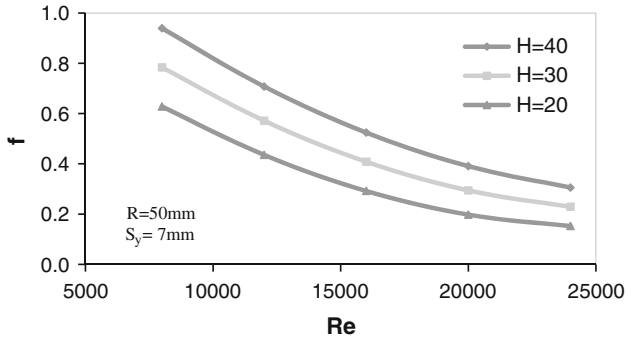

Fig. 12 The effect of Reynolds number on the friction factor at different element heights

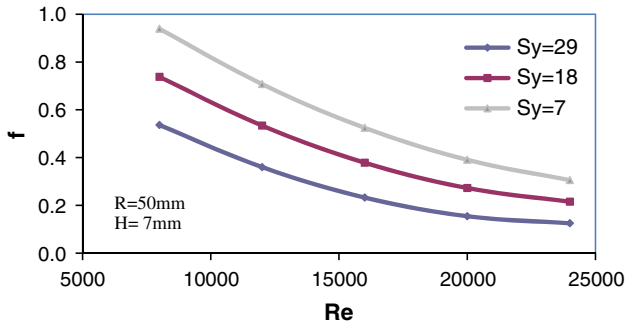

Fig. 13 The effect of Reynolds number on the friction factor at different transverse pitch

increase of the Reynolds number. It is also clear that an increase in the element height (H) leads to an increase in the friction factor (f). The increase of the element height results in a decrease in free flow area, thus blocks the flow more so it leads to an increase in friction factor (f).

The effect of transverse pitch S_y on the friction factor f is presented in Fig. 13. The transverse pitch S_y determinate the dimension of gap among the S-shaped elements. It is clear that an increase in the transverse pitch leads to a decrease in the friction factor f. The increase of the transverse pitch means a decrease in the number of

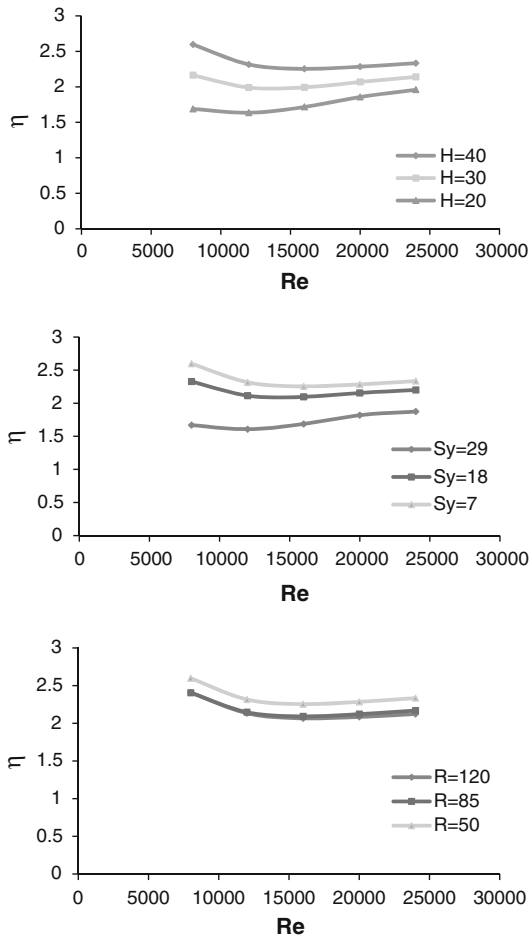

Fig. 14 The effect of design variables on the thermal performance factor

S-shaped element in the channel. The decrease in the number of S-shaped elements disrupts flow less and so it causes a decrease in the friction factor f.

The effect of the element radius R on the friction factor is very small compared to other variables. For this reason it may be stated that there is no effect of the element radius R on the friction factor f.

4.4 Effect of design parameters on the thermal performance factor

According to the results shown above, the S-shaped enhancement elements offers heat transfer rate enhancement in accompany with the increase of friction factor. The increase of friction causes a rise of pumping energy. Therefore, the actual effectiveness of the enhancement elements depends upon the weight of the increase in heat transfer and the increase in friction which can be determined from performance evaluation. Generally, the performance evaluation of the enhancement device is made using the data of the smooth channel as reference and

Table 6 Confirmation tests and their comparison with the results

Exp. no.	Design parameters				Nusselt number (*Nu*)			Friction factor (*f*)		
	H	S_y	R	*Re*	Exp.	Predicted	Error (%)	Exp.	Predicted	Error (%)
1	40	29	50	25,641.75	331.05	340.90	2.89	0.13517	0.12724	−6.24
2	40	29	50	14,658.83	260.38	251.61	−3.48	0.29527	0.26989	−9.41
3	40	18	50	22,209.97	472.29	443.71	−6.44	0.24712	0.23484	−5.23
4	40	18	50	19,585.57	445.11	418.36	−6.39	0.26096	0.28116	7.18
5	40	18	50	17,496.27	418.82	398.18	−5.18	0.30673	0.33311	7.92
					Mean absolute error		4.88	Mean absolute error		7.20

usually considered at the same pumping power, since this is relevant to the operation cost. For constant pumping power

$$\left(\dot{V}\Delta P\right)_s = \left(\dot{V}\Delta P\right)_a \tag{14}$$

where $\dot{V}_s$ and $\dot{V}_a$ are the volumetric flow rates through the channel, and ΔP_s and ΔP_a are the pressure drops without and with S-shaped enhancement element, respectively. The relationship between friction and Reynolds number can be written as

$$\left(f\mathrm{Re}^3\right)_s = \left(f\mathrm{Re}^3\right)_a \tag{15}$$

The thermal performance factor (η) at constant power is defined as the ratio of the convective heat transfer coefficient of the channel with heat transfer enhancement device to the smooth channel, and can be find as follows:

$$\eta = (Nu_e/Nu_o)\Big/(f_e/f_o)^{1/3}. \tag{16}$$

The thermal performance factor results are plotted in Fig. 14. Figure 14a–c shows the effect of the element height, the transverse pitch, and the element radius on the thermal performance factor (η). For a net energy gain, the value of the η must be greater than unity. In other words, for an effective heat transfer enhancement technique, it should have values greater than unity. From Fig. 14, it is apparent that as Reynolds number increases, the thermal performance factor generally decreases for the element height, the transverse pitch, and the element radius. The heat thermal performance factors are higher than unity for all investigated conditions. This means that the use of S-shaped elements leads to an advantage on the basis of heat transfer enhancement. Figure 14 shows also that the thermal performance factor increases with increasing H, decreasing S_y and decreasing R. In other words, for higher thermal performance, a higher element heights, lower transverse pitch, and lower element radius should be preferred.

5 Confirmation experiments

Since the response surface equations were derived from quadratic regression fit, confirmation tests must be performed to verify their validity. Of course, the independent variable values selected for the confirmation test must lie within the ranges for which the formulas were derived. The five confirmation run experiments are performed for the Nusselt number (*Nu*) and the friction factor (f). The data from the confirmation runs and their comparisons with the predicted values for the Nusselt number (*Nu*) and the friction factor (f) are listed in Table 6. The percentage errors are just deviations between experimental data and model, and then multiplied by 100 %. From the analysis of Table 6, it can be seen the percentage error calculated is small. The range of percentage error between the experimental and the predicted value of *Nu* and f lie within −6.44 to 2.89 % and −9.41 to 7.92 %, respectively. The mean absolute error is found to be 4.88 and 7.20 for the Nusselt number and friction factor, respectively. Obviously, this confirms excellent reproducibility of the experimental conclusions.

6 Conclusions

In this work, an experimental study has been made to determine the thermal performance characteristics of *S*-shaped enhancement elements. An effective procedure of response surface methodology (RSM) has been used for modeling thermal performance characteristics. The element height, the transverse pitch, the element radius, and the Reynolds number are chosen as variables to study the thermal performance in terms of the Nusselt number and the friction factor. With the help of the RSM, correlation equations were developed for the Nusselt number and the friction factor. The results of the study can be summarized as follows:

1. The experimental results showed that the use of the S-shaped enhancement elements may lead to heat transfer enhancement. Higher element height, lower transverse pitch, lower element radius, and higher Reynolds numbers are suggested for higher Nusselt number.
2. The experimental results also showed that the use of the S-shaped enhancement elements may lead to an

increase in the friction factor. An increase in the element height H and a decrease in the transverse pitch lead to an increase in the friction factor f.

3. Most effective parameters on the friction factor (*f*) are found to be the element height (H), the transverse pitch (S_y), and Reynolds number (*Re*). The effect of element radius on the friction factor is negligible.
4. The confirmation tests showed that the mean absolute error is 4.88 and 7.20 for the Nusselt number and friction factor, respectively. These experimental findings indicate that the model used in this study is reasonable and accurate and can be used for determining Nusselt Number *Nu* and friction factor f with the limitations of the factors analyzed.
5. For higher thermal performance, a higher element heights, lower transverse pitch, and lower element radius should be preferred.

References

1. Tahat M, Kodah ZH, Jarrah BA, Probert SD (2000) Heat transfers from pin–fin arrays experiencing forced convection. Appl Energy 67(4):419–442
2. Sara ON, Pekdemir T, Yapıcı S, Yılmaz M (2001) Enhancement of heat transfer from a flat surface in a channel flow by attachment of rectangular blocks. Int J Energy Res 25:563–576
3. El-Sayed SA, Mohamed MS, Abdel-latif AM, Abouda AE (2002) Investigation of turbulent heat transfer and fluid flow in longitudinal rectangular-fin arrays of different geometries and shrouded fin array. Exp Therm Fluid Sci 26:879–900
4. Park K, Choi DH (2004) Shape optimization of a plate–fin type heat sink with triangular-shaped vortex generator. KSME Int J 18(9):867–876
5. Park K, Choi DH, Lee KS (2004) Optimum design of plate heat exchanger with staggered pin arrays. Numer Heat Transf Part A 45:347–361
6. Park K, Choi DH, Lee KS (2004) Numerical shape optimization for high performance of a heat sink with pin–fins. Numer Heat Transf Part A 46:909–927
7. Park K, Moon S (2005) Optimal design of heat exchangers using the progressive quadratic response surface model. Int J Heat Mass Transf 48:2126–2139
8. Chiang KT (2007) Modeling and optimization of designing parameters for a parallel-plain fin heat sink with confined impinging jet using the response surface methodology. Appl Therm Eng 27:2473–2482
9. Chiang KT, Chou CC, Liu NM (2009) Application of response surface methodology in describing the thermal performances of a pin–fin heat sink. Int J Therm Sci 48:1196–1205
10. Sahin B, Demir A (2008) Thermal performance analysis and optimum design parameters of heat exchanger having perforated pin fins. Energy Convers Manag 49:1684–1695
11. Sahin B, Demir A (2008) Performance analysis of a heat exchanger having perforated square fins. Appl Therm Eng 28:621–632
12. Jubran BA, Al-Salaymeh AS (1996) Heat transfer enhancement in electronic modules using ribs and "film-cooling-like" techniques. Int J Heat Fluid Flow 17(2):148–154
13. Rodriguez JF, Renaud JE, Wujek BA, Tappeta RV (2000) Trust region model management in multidisciplinary design optimization. J Comput Appl Math 124:139–154
14. Madsen JI, Langyhjem M (2001) Multifidelity response surface approximations for the optimum design of diffuser flows. Optim Eng 2:453–468
15. Kansal HK, Singh S, Kumar P (2005) Parametric optimization of powder mixed electrical discharge machining by response surface methodology. J Mater Process Technol 169:427–436
16. Naceur H, Ben-Elechi S, Batoz JL, Knopf-lenoir C (2007) Response surface methodology for the rapid design of aluminum sheet metal forming parameters. Mater Des 29(4):781–790
17. Choori W, Pattthanamanee W, Manurakchinakorn S (2008) Use of response surface method for the determination of demineralization efficiency in fermented shrimp shells. Bioresour Technol 99(14):6168–6173
18. Xiarchos I, Jaworska A, Traznadel GZ (2008) Response surface methodology for the modeling of copper removal from aqueous solutions using micellarenhanced ultrafiltration. J Membr Sci 321(2):222–231
19. Acherjee B, Misra D, Bose D, Venkadeshwaran K (2009) Prediction of weld strength and seam width for laser transmission welding of thermoplastic using response surface methodology. Opt Laser Technol 41(8):956–967
20. Wang G, Zhao G, Li H, Guan Y (2011) Research on optimization design of the heating/cooling channels for rapid heat cycle molding based on response surface methodology and constrained particle swarm optimization. Expert Syst Appl 38:6705–6719
21. Khalajzadeh V, Heidarinejad G, Srebric J (2011) Parameters optimization of a vertical ground heat exchanger based on response surface methodology. Energy Build 43:1288–1294
22. Subasi A (2010) Heat exchanger optimization with the helping of response surface method. MS Thesis, Mechanical Engineering Department, Ataturk University, Turkey
23. Box G, Wilson K (1951) On the experimental attainment of optimum condition. J R Stat Soc Ser B 13(1):1–45
24. Montgomery DC (1997) Design and analysis of experiment, 4th edn. Wiley, New York
25. Myers RH, Montgomery DH (1995) Response surface methodology: process and product optimization using designed experiments. Wiley, New York
26. Chen TY, Shu TH (2004) Flow structures and heat transfer characteristics in fan flows with and without delta-wing vortex generators. Exp Therm Fluid Sci 28(4):273–282
27. Ozisik MN (1985) Heat transfer: a basic approach. McGraw-Hill Int Ed, Boston
28. Kline SJ, McClinctock FA (1953) Describing uncertainties in single sample experiments. Mech Eng 75:3–8
29. Sara ON, Pekdemir T, Yapici S, Yilmaz M (2001) Heat-transfer enhancement in a channel flow with perforated rectangular blocks. Int J Heat Fluid Flow 22:509–518